

High-Temperature Fatigue Crack Growth Behavior of 17-4 PH Stainless Steels at Various Load Ratios

C.-K. Lin, K.-C. Hsu

*Department of Mechanical Engineering, National Central University,
Jhong-Li 32001, Taiwan*

The high-temperature fatigue crack growth (FCG) behavior at 400 and 500°C was investigated for variously heat-treated 17-4 PH stainless steels under different load ratios. Results indicated the FCG rates (FCGRs) at 400°C increased with R -ratio at the low ΔK regime and merged together at the high ΔK regime for all the given heat-treated conditions, except for a peak-aged condition. At 500°C, the FCGRs of the given alloys increased with R -ratio at low R -ratios and became comparable at high R -ratios. The variations of FCGR with R -ratio could be described as an intrinsic FCG behavior based on a Unified Approach. Accordingly, the predominant FCG mechanism was similar to a general plastic blunting process except for the high R -ratio regime of the peak-aged condition tested at 400°C.

1. Introduction

As a type of martensitic precipitation-hardening stainless steel, 17-4 PH alloy has been used extensively in various applications, such as nuclear, chemical, aircraft, and naval industries [1]. A wide range of mechanical properties can be obtained for the 17-4 PH stainless steel through suitable heat treatments in the temperature range of 482-621°C (900-1150°F) [1-6]. Maximum strength and hardness values are generally obtained after aging at 450-510°C, during which coherent copper-rich precipitate clusters are formed [1-3]. Aging at higher temperatures (above 540°C) leads to formation of large, incoherent copper-rich precipitates which result in a lower strength and hardness and an enhancement of toughness [1-3]. As many applications of the 17-4 PH stainless steel are involved with high temperatures, it is important to characterize the high-temperature fatigue behavior of the 17-4 PH alloy to better predict the service life of components made from this material. Although there are some studies [7-11] focused on the high-temperature fatigue behavior of 17-4 PH stainless steels, there is lack of consideration of the effects of load ratio (R -ratio, $R = P_{\min}/P_{\max}$) on the fatigue crack growth (FCG) behavior of such steels. As part of a series of studies on the high-temperature fatigue and mechanical properties of 17-4 PH stainless steels [7-12], the aim of this study is to investigate the influence of R -ratio on the high-temperature FCG behavior of such alloys at 400 and 500°C.

2. Experimental Procedures

The 17-4 PH stainless steels used in the present work were supplied by the vendor in the form of hot-rolled, solution-annealed plates. The chemical composition of

this steel in wt% is 15.18 Cr, 4.47 Ni, 3.47 Cu, 0.65 Mn, 0.38 Si, 0.2 (Nb + Ti), 0.15 Mo, 0.03 S, 0.02 C, 0.016 P, and balance of Fe. Three different types of heat treatments were applied to the specimens, namely as-received “Condition A,” peak-aged “Condition H900,” and overaged “Condition H1150.” For Condition A, specimens were heated to 1038°C (1900°F), held for 0.5 h and cooled to room temperature in air. For Conditions H900 and H1150, specimens were first heat treated as in Condition A and then aged at 482°C (900°F) for 1 h or 621°C (1150°F) for 4 h, respectively, followed by air cooling. Condition H900 has the greatest strength and hardness but also has the least ductility, while Condition H1150 shows the least strength but greatest ductility among the given three conditions. Details of the mechanical properties at room and high temperatures for these three heat treatments can be found in [7,12].

FCG tests were carried out on a commercial closed-loop servo-hydraulic test machine at temperatures of 400 and 500°C in laboratory air. A commercial two-zone, SiC-heated furnace was used to heat the specimens. FCG tests were performed according to ASTM E647 under constant load control with a triangular loading waveform at a frequency of 2 Hz and *R*-ratios ranging from 0.1 to 0.7. Pin-loaded single-edge-notched-tension (SENT) specimens with a 25.4-mm width, 3-mm thickness and 6.35-mm-deep notch were used. Geometry of the specimen and the formula in determination of the stress intensity factor for such a geometry was given in [10]. Crack length during each test was measured by a direct-current potential drop (DCPD) technique. Details of the experimental setup, FCG testing technique, and determination of fatigue crack growth rate (FCGR) can be found in [10]. Scanning electron microscopy (SEM) was used for characterization of the fracture surface.

3. Results and Discussion

3.1 Effects of *R*-ratio on fatigue crack growth rate

Comparisons of FCGR curves under different *R*-ratios (from 0.1 to 0.7) at 400 and 500°C are shown in Fig. 1 for variously heat-treated 17-4 PH stainless steels. Note that in Fig. 1, ΔK is the applied stress intensity factor range. Only the FCGR curves at selected *R*-ratios are shown in Fig. 1 for the sake of clarity but still represent the general trends. In addition, since the FCG behavior of Conditions A and H900 was similar to that of H1150 at 500°C [10,11], only Condition H1150 was representatively tested at 500°C. The comparable FCG behavior at 500°C for all the given heat-treated conditions was mainly caused by an in-situ overaging and precipitate-coarsening effect during test for Conditions A and H900, respectively, as described and confirmed previously [10,11]. In Fig. 1, it can be seen that for all the given heat-treated conditions, the FCGRs at 400°C were increased with *R*-ratio at the lower ΔK regime. This can also be seen as a shift of the FCG threshold to the left when the *R*-ratio was increased. For Conditions A and H1150 at 400°C (Figs. 1(a) and (c)), the differences in FCGR among various *R*-ratios were decreased with increasing ΔK and eventually the curves merged

together at the higher ΔK regime, especially for those at higher R -ratios ($R \geq 0.3$). A similar trend was observed for FCGRs of Condition H900 at 400°C (Fig. 1(b)) under $R \leq 0.5$, but the FCGRs were increased again with R -ratio at higher R -ratios ($R > 0.5$) for the entire ΔK regime. For Condition H1150 at 500°C (Fig. 1(d)), the FCGRs were increased with R -ratio at lower R -ratios ($R \leq 0.3$) for the entire ΔK regime and became comparable with each other at higher R -ratios ($R \geq 0.3$).

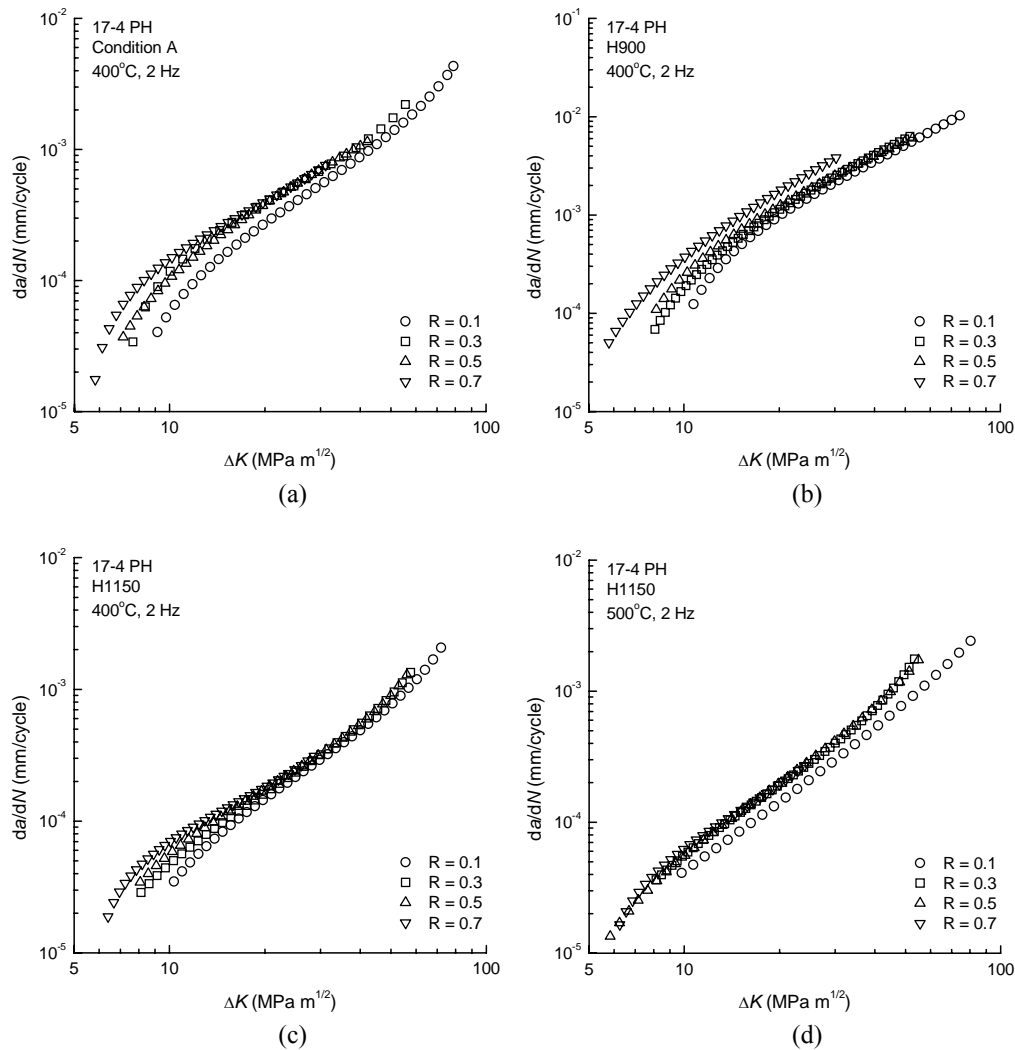


Fig. 1 Comparisons of FCGR curves under different load ratios at 400 and 500°C.

An approach, called the “Unified Approach,” for considering the effect of R -ratio on FCG behavior was applied to describe the FCG behavior observed in the current study. Such an approach has been described in many studies by Vasudevan, Sadananda, and co-workers (e.g., [13-19]). It is assumed that for a fatigue crack to advance at a certain crack growth rate, two critical stress intensity factor values should be met simultaneously. These values are a critical stress

intensity factor range, ΔK^* , and a critical maximum stress intensity factor, K_{\max}^* . The requirement of ΔK^* indicates a need of a cyclic load to induce fatigue damage ahead of the crack tip, while the requirement of K_{\max}^* allows the maximum load to break the crack tip bands in a cyclically damaged region for crack to propagate [13]. According to the description, a critical R -ratio, R^* , can be defined as follows:

$$R^* = 1 - (\Delta K^* / K_{\max}^*) \quad (1)$$

in which both ΔK and the maximum applied stress intensity factor, K_{\max} , have the critical minimum values at this R -ratio. For R -ratios higher than the critical value ($R > R^*$), K_{\max} must be increased to meet the critical stress intensity factor range, ΔK^* , and the values of ΔK and K_{\max} can be described in the following:

$$\begin{aligned} \Delta K &= \Delta K^* \\ K_{\max} &= \Delta K^* / (1 - R) \end{aligned} \quad (2)$$

On the other hand, when the R -ratio is below the critical value ($R < R^*$), ΔK must be increased to meet the critical maximum stress intensity factor, K_{\max}^* , and the values of ΔK and K_{\max} can be described as follows:

$$\begin{aligned} \Delta K &= K_{\max}^* (1 - R) \\ K_{\max} &= K_{\max}^* \end{aligned} \quad (3)$$

Thus, the variation of ΔK and K_{\max} with R can be described as an intrinsic behavior using ΔK^* and K_{\max}^* (Eqs. (1)-(3)). In addition, the relationship between ΔK^* and K_{\max}^* along the variation of crack growth rate reflects the characteristics of crack growth mechanism, i.e., changes of the contribution from the cyclic and monotonic portions in the crack growth process [15].

To determine the critical stress intensity factor values for a given testing condition, the ΔK and K_{\max} values corresponding to a certain FCGR at all R -ratios are present in terms of ΔK vs. K_{\max} . The data points in this type of plot would show an L-shape curve and the asymptotic limits of the L-shape curve indicate the critical values of ΔK and K_{\max} , namely ΔK^* and K_{\max}^* , respectively, corresponding to the selected FCGR [13]. By plotting this type of curve at selected FCGRs, the corresponding ΔK^* and K_{\max}^* values and the relationship between these two critical stress intensity factors along the variation of crack growth rate could be known [15].

In the current study, the FCGRs in the Paris region (Region II) of each testing condition were chosen and the corresponding ΔK and K_{\max} values at all given R -ratios were plotted in terms of ΔK vs. K_{\max} to get the ΔK^* and K_{\max}^* values. For Conditions A and H1150 at 400°C and Condition H1150 at 500°C, L-shape curves in such plots could be clearly defined and the ΔK^* and K_{\max}^* values were

determined without difficulties. Representative L-shape curves of Condition A at 400°C are shown as examples in Fig. 2. Note that each point in the plot as seen in Fig. 2 represents a specific FCGR. However, for Condition H900 at 400°C, deviations of data points from the L-shape curves at the higher R -ratio regime ($R = 0.6$ and 0.7) were observed, as shown in Fig. 3. As specified by the Unified Approach, data points deviated from the L-shape curve indicate that a different crack growth mechanism might take place at that specific regime [19]. The FCGR data for Condition H900 at 400°C can then be divided into two regions, $R = 0.1-0.5$ and $R \geq 0.6$, with each region having an individual crack growth mechanism with its own ΔK^* and K_{\max}^* [19]. Therefore, the FCG behavior of Condition H900 at 400°C was thought to have two controlling crack growth mechanisms, one dominating at the low R -ratio regime and the other dominating at the high R -ratio regime. In this regard, the ΔK^* and K_{\max}^* values for the low R -ratio regime of Condition H900 at 400°C were determined by using the aforementioned procedures with the data of $R = 0.1-0.5$. However, due to the limited data points at $R = 0.6$ and 0.7 , the ΔK^* and K_{\max}^* values for the high R -ratio regime of Condition H900 at 400°C could not be completely determined.

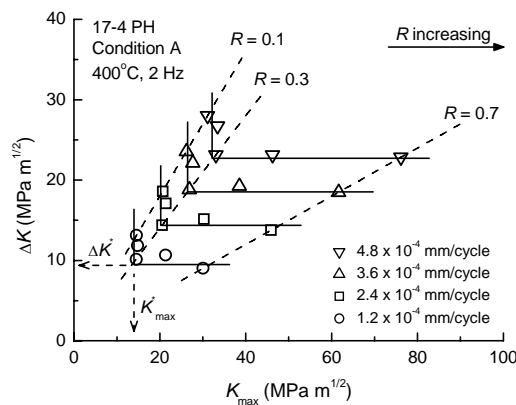


Fig. 2 ΔK vs. K_{\max} at certain FCGRs for Condition A at 400°C, 2 Hz and all given R -ratios.

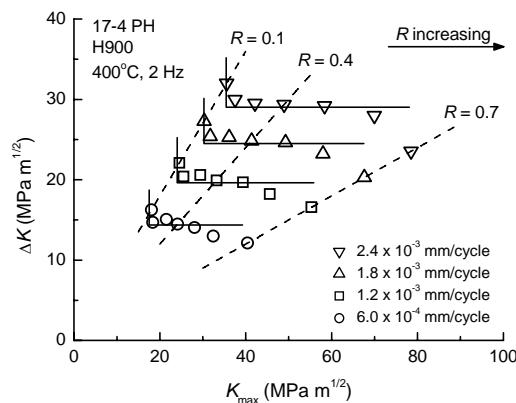


Fig. 3 ΔK vs. K_{\max} at certain FCGRs for Condition H900 at 400°C, 2 Hz and all given R -ratios.

3.2 Effects of R-ratio on fatigue crack growth mechanism

The ΔK^* and K_{\max}^* values calculated using the procedures described above for the given testing conditions are present as ΔK^* vs. K_{\max}^* in Fig. 4. Note that each point in Fig. 4 represents a specific FCGR. This type of figure is called “trajectory map” of crack growth, since trajectories of the relationship between the two critical driving forces for crack growth, ΔK^* and K_{\max}^* , are shown and can be used as a map to interpret the crack growth mechanisms [15]. In a general trajectory map, the path of $\Delta K^* = K_{\max}^*$ (the dash line in Fig. 4) is called the “ideal fatigue line” [15] indicating a pure cycle-controlling crack growth mechanism such as the plastic blunting mechanism [20] in polycrystalline materials. Trajectories deviating from the ideal fatigue line indicate a change of crack growth mechanism and most of the deviations occur when a predominant K_{\max} -controlling mechanism is involved [15].

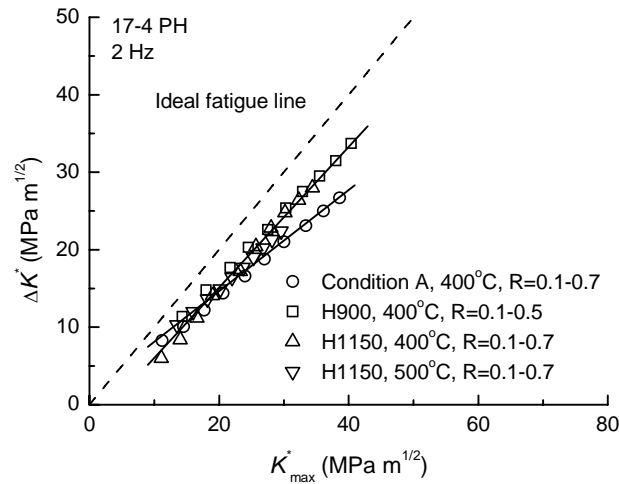


Fig. 4 Crack growth trajectory map for all given testing conditions.

As shown in Fig. 4, the crack growth trajectories for Condition H1150 at 400 and 500°C and for the low R -ratio regime ($R = 0.1-0.5$) of Condition H900 at 400°C were almost the same. This implies that the FCG behavior in these conditions was controlled by a similar mechanism. Trajectories for these conditions were parallel to the ideal fatigue line and located underneath the ideal fatigue line. This indicates that the contribution of K_{\max} was slightly greater than that of ΔK to the specific crack growth mechanism and the extent of contribution was constant with increasing K_{\max} . It has been found in a previous study [11] that for all the given three heat-treated 17-4 PH alloys tested at 400 and 500°C with $R = 0.1$ and a frequency of 2 Hz, the environment had an insignificant effect on the FCG mechanism. Creep or oxidation mechanism was not found to substantially assist the FCG under these conditions and the difference in FCGR among the various heat treatments was attributed to a difference in the extent of intensity of planar slip at the crack tip [11]. The controlling crack growth mechanisms for these

given testing conditions were alike and presumably similar to a general plastic blunting process [20]. It is therefore not surprising to see that the trajectories for these conditions are merged to a line parallel to the ideal fatigue line. Note that the differences in FCGR could not be shown in the trajectory map; similar trajectories only indicate similar crack growth mechanisms but not similar FCGRs. Therefore, such converged trajectories for Condition H1150 at 400 and 500°C and for the low R -ratio regime of Condition H900 at 400°C presumably represent a baseline crack growth mechanism of 17-4 PH alloy at high temperature.

As described above, a different crack growth mechanism might take place at the high R -ratio regime ($R = 0.6$ and 0.7) of Condition H900 at 400°C. A true trajectory for this regime could not be drawn in Fig. 4 due to limited data points. However, if the critical load ratio were set equal to 0.7 for the high R -ratio regime of Condition H900 at 400°C, the data of $R = 0.6$ and 0.7 could then be used to find a virtual $\Delta K^* - K_{\max}^*$ trajectory. It would be expected that this virtual trajectory would be significantly deviated from the ideal fatigue line and located much closer to the K_{\max}^* -axis, as compared to those trajectories given in Fig. 4. The expecting trend of this virtual trajectory provides a clue that there might exist a superimposed monotonic fracture mode at a higher K_{\max} [15,18]. The proposed monotonic fracture mode for the current case is a crystallographic-faceted mode, in which K_{\max} plays a major role [15]. FCG occurs crystallographically along slip planes in the faceted mode, particularly in planar-slip materials [21]. As a peak-aged condition that contains coherent precipitates in the matrix, Condition H900 has the highest intensity of planar slip among the three given heat-treated conditions tested at 400°C [10,11,22]. Features of the crystallographic-faceted fracture mode were indeed observed on the fracture surfaces of high-load-ratio specimens of Condition H900 at 400°C, as exemplified in Fig. 5. Therefore, the crystallographic-faceted fracture mode was considered as the primary crack growth mechanism for Condition H900 at 400°C under high R -ratios. Such a fracture surface morphology was somewhat different from that of Condition H1150 tested at 400 and 500°C, as exemplified in Fig. 6. Note that the crack growth direction in both Figs. 5 and 6 is from left to right.

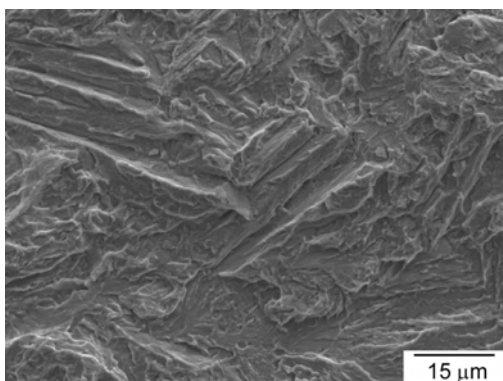


Fig. 5 SEM micrograph of the fracture surface for Condition H900 tested at 400°C, 2 Hz, and $R = 0.6$.

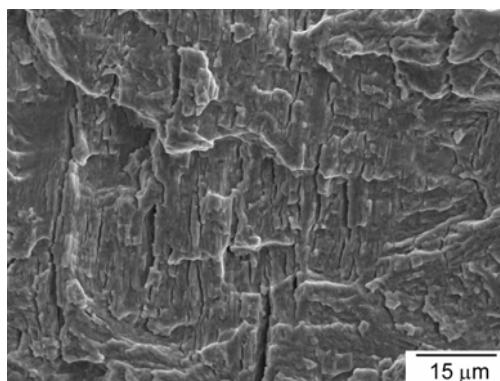


Fig. 6 SEM micrograph of the fracture surface for Condition H1150 tested at 400°C, 2 Hz, and $R = 0.3$.

As shown in Fig. 4, the trajectory for Condition A at 400°C was progressively deviated from the ideal fatigue line with an increase in K_{\max}^* . Its lower slope value suggests an increasing influence of a K_{\max} -controlling mechanism at high K_{\max} . In addition, the upper portion of this trajectory is located below those of Condition H1150 at 400 and 500°C and the low R -ratio region of Condition H900 at 400°C, as shown in Fig. 4. It was found that when tested at 400°C, Condition A would undergo an in-situ precipitation-hardening process and the FCG behavior would become closer to that of Condition H900 [10,11]. Thus, a similar influence of the crystallographic-faceted fracture mode on the FCG behavior of Condition H900 at the high R -ratio regime was also expected to occur in Condition A at 400°C. The degree of similarity in FCG behavior between Conditions A and H900 at 400°C was determined by the testing time of Condition A [11]. Since the time needed for Condition A to complete the precipitation-hardening process at 400°C is longer than the testing time at 2 Hz [11,12], the influence of the crystallographic-faceted fracture mode on the FCG behavior of Condition A would not be so pronounced as that for Condition H900. In this regard, a slightly deviated trajectory from the baseline (that for Conditions H1150 at 400 and 500°C and the low R -ratio region of Condition H900 at 400°C) was observed for Condition A tested at 400°C with a loading frequency of 2 Hz.

4. Conclusions

- (1) For all the given 17-4 PH stainless steels tested at 400°C, the FCGRs increased with R -ratio at lower ΔK values and became comparable at the higher ΔK region, except for Condition H900, under which FCGRs increased with R -ratio throughout the applied ΔK region. For all the given testing conditions at 500°C, the FCGRs increased with R -ratio at lower R -ratios and merged together at higher R -ratios for the entire ΔK regime.
- (2) The variations of FCGR with R -ratio could be described as an intrinsic behavior of FCG based on a Unified Approach. The essential high-temperature FCG mechanism for all the given 17-4 PH alloys was presumably a typical plastic blunting process, except for Condition H900 tested at 400°C with high R -ratios, in which a crystallographic-faceted fracture mode played an important role.

Acknowledgement

This work was funded by the National Science Council (Taiwan) under Contract No. NSC-91-2216-E-008-007.

References

- [1] W.F. Smith, *Structure and Properties of Engineering Alloys*, 2nd ed., McGraw-Hill Inc., New York, 1993.
- [2] U.K. Viswanathan, S. Banerjee, R. Krishnan, Effect of aging on the microstructure of 17-4 PH stainless steel, *Mater Sci Engng A* 104 (1988) 181-189.
- [3] H.J. Rack, D. Kalish, The strength, fracture toughness, and low cycle fatigue behavior of 17-4 PH stainless steel, *Metall Trans* 5 (1974) 1595-1605.
- [4] F.B. Pickering, Physical metallurgy of stainless steel developments, *Int Met Rev* (21) 1976 227-268.
- [5] R.D.K. Misra, G.Y. Prasad, T.V. Balasubramanian, P.R. Rao, Effect of phosphorus segregation on impact toughness variation in 17-4 PH precipitation hardened stainless steel, *Scr Metall* 20 (1986) 713-716.
- [6] R.D.K. Misra, G.Y. Prasad, T.V. Balasubramanian, P.R. Rao, On variation of impact toughness in 17-4 PH precipitation hardened stainless steel, *Scr Metall* 21 (1987) 1067-1070.
- [7] J.-H. Wu, C.-K. Lin, Tensile and fatigue properties of 17-4 PH stainless steel at high temperatures, *Metall Mater Trans* 33A (2002) 1715-1724.
- [8] J.-H. Wu, C.-K. Lin, Influence of frequency on high-temperature fatigue behavior of 17-4 PH stainless steels, *Mater Trans* 44 (2003) 713-721.
- [9] J.-H. Wu, C.-K. Lin, Effect of strain rate on high-temperature low-cycle fatigue of 17-4 PH stainless steels, *Mater Sci Engng A* 390 (2005) 291-298.
- [10] K.-C. Hsu, C.-K. Lin, High-temperature fatigue crack growth behavior of 17-4 PH stainless steels, *Metall Mater Trans* 35A (2004) 3018-3024.
- [11] K.-C. Hsu, C.-K. Lin, Influence of frequency on the high-temperature fatigue crack growth behavior of 17-4 PH stainless steels, *Mater Trans* 48 (2007) 490-499.
- [12] J.-H. Wu, C.-K. Lin, Influence of high temperature exposure on the mechanical behavior and microstructure of 17-4 PH stainless steel, *J Mater Sci* 38 (2003) 965-971.
- [13] A.K. Vasudevan, K. Sadananda, N. Louat, Two critical stress intensities for threshold fatigue crack propagation, *Scr Metall Mater* 28 (1993) 65-70.
- [14] A.K. Vasudevan, K. Sadananda, Fatigue crack growth in metal matrix composites, *Scr Metall Mater* 28 (1993) 837-842.
- [15] K. Sadananda, A.K. Vasudevan, R.L. Holtz, Extension of the unified approach to fatigue crack growth to environmental interactions, *Int J Fatigue* 23 (2001) S277-S286.
- [16] A.K. Vasudevan, K. Sadananda, Analysis of fatigue crack growth under compression-compression loading, *Int J Fatigue* 23 (2001) S365-S374.

- [17] K. Sadananda, A.K. Vasudevan, Fatigue crack growth mechanisms in steels, *Int J Fatigue* 25 (2003) 899-914.
- [18] K. Sadananda, A.K. Vasudevan, I.W. Kang, Effect of superimposed monotonic fracture modes on the ΔK and K_{max} parameters of fatigue crack propagation, *Acta Mater* 51 (2003) 3399-3414.
- [19] K. Sadananda, A.K. Vasudevan, Multiple mechanisms controlling fatigue crack growth, *Fatigue Fract Engng Mater Struct* 26 (2003) 835-845.
- [20] C. Laird, The influence of metallurgical structure on mechanics of fatigue crack propagation, in: *Fatigue Crack Propagation*, ASTM STP 415, American Society for Testing and Materials, Philadelphia, 1967, pp. 131-169.
- [21] K. Sadananda, P. Shahinian, Analysis of crystallographic high temperature fatigue crack growth in a nickel based alloy, *Metall Trans* 12A (1981) 343-351.
- [22] E.A. Starke, Jr., G. Lutjering, Cyclic plastic deformation and microstructure, in: *Fatigue and Microstructure*, American Society for Metals, Metals Park, Ohio, 1978, pp. 205-243.